PCCP

Graphene-Covered Transition Metal Halide as Efficient and Durable Electrocatalysts for Oxygen Reduction and Evolution Reactions

Journal:	*Physical Chemistry Chemical Physics*
Manuscript ID	CP-ART-08-2019-004618.R1
Article Type:	Paper
Date Submitted by the Author:	26-Sep-2019
Complete List of Authors:	Zhang, Detao; Beijing University of Chemical Technology Zhang, Jing; Northwestern Polytechnical University Gong, LeLe; East China University of Technology Zhu, Yonghao; Beijing University of Chemical Technology Zhang, Lipeng; Beijing University of Chemical Technology Xia, Zhenhai; University of North Texas

ARTICLE

Graphene-Covered Transition Metal Halide Molecules as Efficient and Durable Electrocatalysts for Oxygen Reduction and Evolution Reactions

Received 00th January 20xx,
Accepted 00th January 20xx

DOI: 10.1039/x0xx00000x

Detao Zhang[a], Jing Zhang[b], Lele Gong[a], Yonghao Zhu[a], Lipeng Zhang[a*], and Zhenhai Xia[c*]

Proton exchange fuel cells (PEFC) are one of the most popular and promising energy conversion devices because of their highly stable and efficient membranes in acidic media, but there is lack of durable non-noble metal electrocatalysts suitable for the acidic environments. Herein, we designed a new type of electrocatalysts consisting of transition metal halide molecules covered by graphene sheets, which is supported by the experiments. To rapidly screen the best catalysts from numerous candidate materials, the electronic structures, reaction free energies and overpotentials of those graphene-covered halide catalysts were studied by the first-principles calculations to predict the catalytic activities for oxygen reduction reaction (ORR) and oxygen evolution reaction (OER). An intrinsic descriptor, the electrostatic force induced by the metallic ions, was found to well describe the catalytic activities and provides a better understanding of the local electrical field effects on catalytic activities. The spin-down d-band center was also introduced to describe catalytic activities of the catalysts. The results demonstrate that the graphene-covered $CrBr_2$ shows the best bifunctional catalytic activities for fuel cells while graphene-covered CoF_2 could well facilitate H_2O_2 production. These catalysts are better than the best commercial noble metal catalysts (e.g., Pt and RuO_2) in terms of overpotentials and activities. This work provides a theoretical base for rationally designing durable electrocatalysts with excellent catalytic activities.

1. Introduction

Clean energy conversion such as hydrogen fuel to electricity by fuel cells and energy storage through metal-air batteries are considered as critical emerging technologies to replace traditional fossil fuels. In these energy technologies, oxygen reduction reaction (ORR) and oxygen evolution reaction (OER) are two key reactions that determine conversion efficiency, and electrocatalysts are usually needed to promote those reactions [1]. Among the traditional electrocatalysts, noble metal catalysts are often applied to catalyse the ORR and OER (e.g., Pt for ORR[2], and RuO_2 for OER[3]). However, the high cost and limited resources of the noble metals hinder their large-scale commercial application of the energy technologies [1].

In the past decades, nonprecious metal and metal-free catalysts have been developed to preplace or reduce the use of noble metal catalysts. In particular, metal-free catalysts, such as nitrogen doped carbon nanotubes and graphene, performed much better ORR catalytic activity than Pt [4]. Multitudinous carbon catalysts, including heteroatom (e.g., B, N, F, O, S, P and transition metals) doped graphene, carbon dots, carbon nitride, graphite, and defective graphene were also developed for efficient electrocatalysts [5-10]. However, those carbon-based electrocatalysts, like nonprecious metal catalysts, still suffer from poor durability, in particular in acid media although most of them works well in alkaline environments. This downgrade the proton exchange fuel cells (PEFC), the most popular and promising ones in commercial applications because of their highly stable and efficient membranes in acidic media. It is therefore necessary to develop electrocatalysts well suitable for acidic environments.

[a] College of Energy, Beijing University of Chemical Technology, Beijing, 100029, China.
[b] School of Materials Science and Engineering, Northwestern Polytechnical University, Xi'an, Shaanxi 710072, China.
[c] Department of Materials Science and Engineering, University of North Texas, Denton, TX 76203, USA.
* Correspondence authors. Zhanglipeng2011@gmail.com, Zhenhai.xia@unt.edu
Electronic Supplementary Information (ESI) available: [details of any supplementary information available should be included here]. See DOI: 10.1039/x0xx00000x

Apart from the doping in graphene, intermolecular charge-transfer via non-covalent functionalization has also been demonstrated to enhance ORR electrocatalytic activities of graphene. The non-covalent functionalization involves weak interactions, which cause no change on the basal plane structure of graphene and its electronic properties being largely retained.[11] The enhanced electrocatalytic activities originate from the intermolecular charge transfer between the undoped graphene and physically adsorbing polarized organic molecules (e.g., poly(diallyl dimethylammonium chloride) (PDDA), and Tetracyanoethylene (TCNE)) on the basal plane of pristine graphene sheets.[11-13] This "intermolecular charge-transfer" offers a simple, low-cost approach to develop carbon-based metal-free ORR catalysts. However, these adsorbed organic molecules still suffer from the acidic attack in the acidic environments, which reduces the stability of the catalysts.

In this paper, we designed novel electrocatalysts consisting of graphene sheets embedded with transition metal halide molecules. Graphene is extremely flexible with large surface area, excellent mechanical and electrical properties, and highly stable in fuel cell environments, while halide molecules are polarized and could be embedded into the graphene sheets [14,15]. While the halide molecules are covered and separated from the reactive environment by the graphene, their high polarization would enhance the catalytic activity through spin or charge transfer between the graphene and the halide molecules. Such graphene-covered halide catalysts would be durable while having highly catalytic activity in acidic environments.

The above new catalyst design involves the selection of catalysts from numerous candidate materials. However, experimentally searching for the best catalysts would be time-consuming and costly. In contrast, computational approaches could be used to rapidly screening of the best catalysts, and provide the guidelines to the experiment. Recently computational and theoretical methods were used to elucidate the microscopic details underlying the mechanisms of operation behind the functioning of PEFC. [16-18] Activity descriptors were developed to identify the best ORR/OER catalysts for heteroatom-doped carbon nanomaterials and covalent organic framework (COF). [19,20] In this work, DFT calculation method will be used to establish a design principle to guide the structural design for the family of graphene-halide catalysts.

2. Simulation methods

Transition metal (TM) halide (TMX_2) absorbed graphene (G) sheets were constructed to calculate their catalytic performances (TM = Ti, V, Cr, Mn, Fe, Co, Ni, Cu, Zn, and X = F, Cl, Br, I). The TMX_2 molecules we studied are listed in Table S1. Such graphene structures embedded with salts have been achieved experimentally.[14,15,21] As illustrated in Figure 1, the unit cells of the structures used in this study are composed of a single-layer graphene sheet adsorbed with a metal halide molecule, the size of which was set to 12.82 Å × 9.87 Å × 20Å. The Van der Waals correction was also taken into consideration in the calculations. Gaussian smearing method was used to determine the electronic partial occupancies. In this design, only graphene surface is exposed to the reactants while the halides are hided behand the graphene. The G/TMX_2 was constructed as a three-dimensional periodic structure, where the vacuum layer was set to be around 20 Å in the z-directions to avoid interaction between slabs.

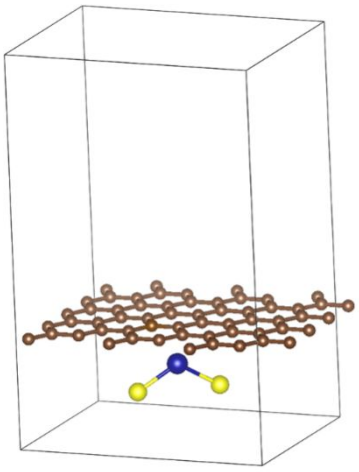

Figure1. The unit cell model of TMX_2 adsorbed graphene. The brown, yellow and blue atoms represent Carbon, Halogen, and TM, respectively.

The free energies and overpotentials of OER and ORR on the structures were calculated with the density functional theory (DFT) method, the Vienna Ab initio Simulation Package (VASP) [22,23]. The Perdew-Burke-Ernzenhof (PBE) exchange correlation functional and soft projector-augmented wave (PAW) pseudopotentials were implemented in VASP code via the DFT. [24,25]. The PBE functional which in our previous studies

have been shown a great performance of the carbon based system.[19,20] For 3d transition metals in this work, DFT+U methods [26] were also considered in the calculations, and the values of U-J are listed in Table S2. The cut off energy of plane wave basis was set 550 eV, and the structures were sampled by 3×3×1 Monkhorst-Pack k-point mesh. Both the cutoff energy and k point meshes were converged within 1 meV in per atom. The whole calculations in spin-polarized with the lowest energy magnetic configurations were identified for all the surfaces and the geometries were relaxed until a maximum force of 0.01 eV /Å was converged.

3. Results and Discussion

3.1 Electronic structures and reaction pathways

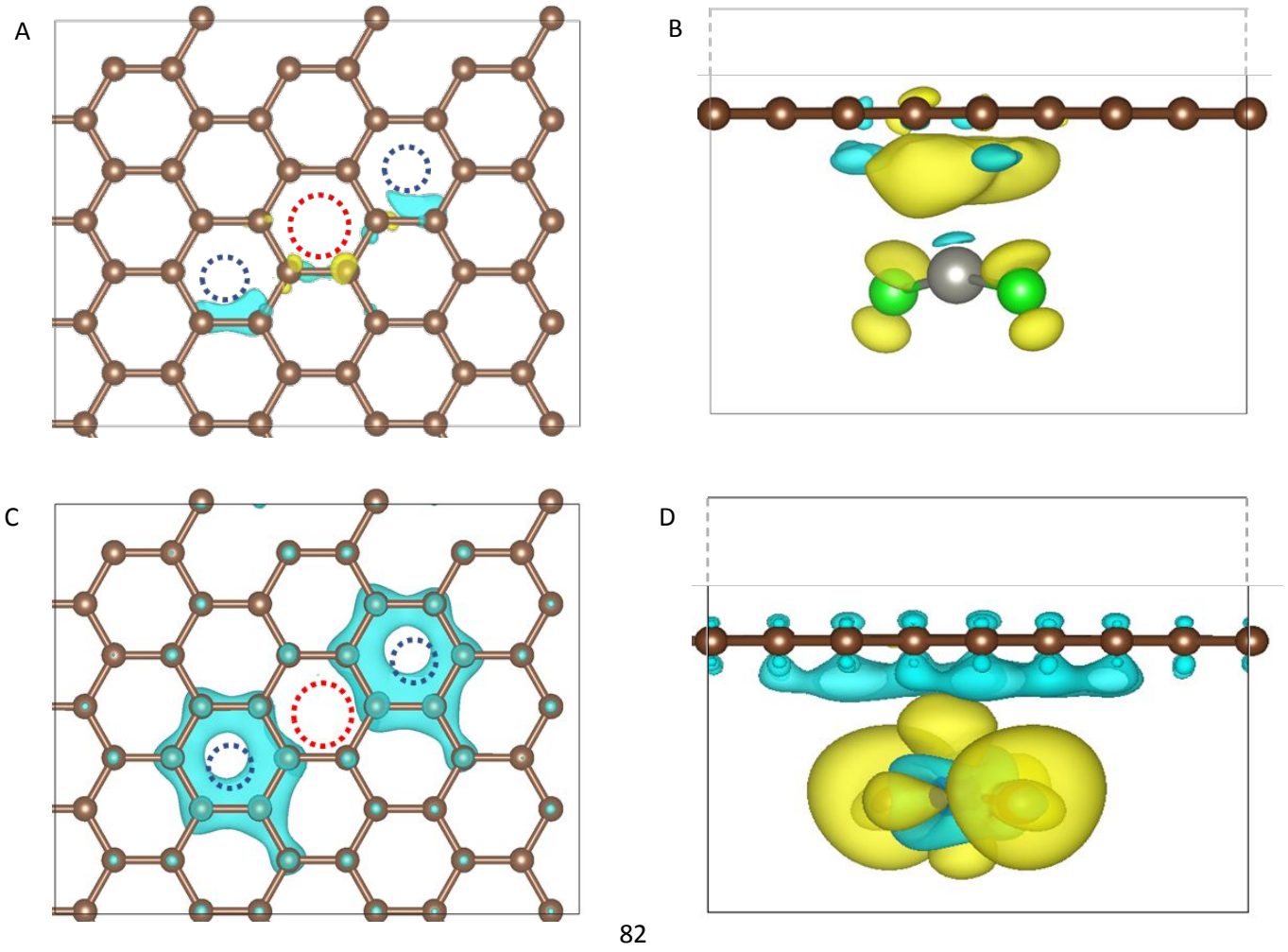

Figure 2. Differential charge density distribution on the graphene absorbed with $ZnBr_2$ (no charge transfer between the graphene and $ZnBr_2$) in (A) top view and (B) side view. The gray and red dotted cycles represent Br and Zn, respectively. Differential charge density distribution on the graphene absorbed with $CoBr_2$ with a charge transfer between the graphene and $CoBr_2$ (0.78e) in (C) top view and (D) side view. The gray and red dotted cycles represent Br and Co, respectively. The blue and yellow colors indicate the positive and negative values of electron quantities, respectively. The isosurface level is 0.0005.

The electronic structures, the electron transfer between TMX_2 and graphene, and the effect of electronic field on ORR and OER were calculated by the DFT. Both 2 and 4-electron pathways of OER and ORR (Supplementary information) and reaction free energy were analyzed following the approaches described in references.[3,27-33] Figure S1 shows the optimized configurations of the G/TMX_2 and Bader differential charge density distribution on the graphene with the largest and smallest Bader charge transfer of every group. Figure 2A and B shows optimized structures and Bader differential charge density distribution of $G/ZnBr_2$ with zero charge transfer while Figure 2 C and D shows optimized structures and Bader differential charge density distribution of $G/CoBr_2$ with the largest charge transfer (0.78e) among G/TMX_2. The metal ions are highly positively charged, while the charge on the graphene redistributes near the halide molecule. In addition, there exists electron transfer between the TMX_2 molecules and graphene. The charge transfer could be positive, negative or zero, depending on the type of the metal ions in halides (Table S1 and S3). Thus, the adsorption of TMX_2 induces charge redistribution on graphene as well as

the charge transfer. The highly positively charged ions, charge transfer and charge redistribution may have a strong effect on the catalytic activities.

The catalytic activities of G/TMX_2 were evaluated by calculating the minimum overpotential of ORR and OER on the graphene surface. The overpotential η of ORR/OER has been considered as an important measure of the catalytic activities of catalysts[2]. For an ideal ORR/OER catalyst, it should promote the OER/ORR just above the equilibrium potential, with zero overpotential[2]. However, since the binding energies of the intermediates are correlated, this perfect state cannot be achieved. Thus, the lower the overpotential, the better the catalysts.

To find out the lowest overpotentials of active sites on the $G/TMBr_2$, we calculated the free energy of the four elementary steps of OER/ORR on all the possible sites that could occur on the graphene. Because the four elementary steps are correlated with each other, we analyzed the adsorption energies of the HOO*, OH*, and O* intermediates adsorbed on graphene during ORR and OER（Table S4 and S5). Figure 3A illustrates the catalytic cycle of ORR in 4-electron pathway (A-B-C-D-A) and 2-electron pathways (A-E-A). In 2-electron transfer pathways, we only analyzed the HOO* (Table S6）for it is the only intermediate in this reaction.

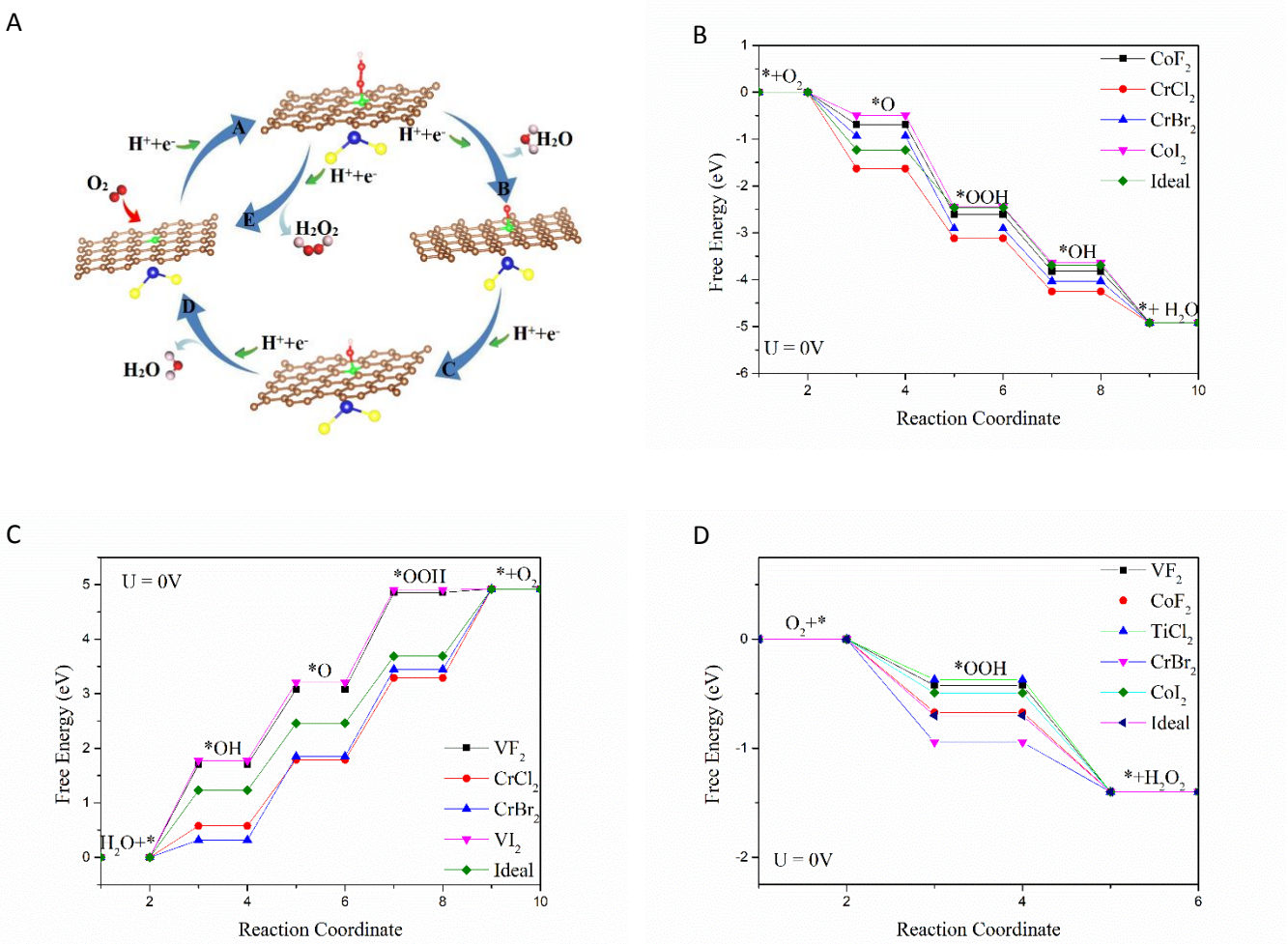

Figure 3. (A) Schematics of ORR cycles on the active site of halide-adsorbed graphene in 4- and 2-electron transfer pathways. The green atom on graphene represents an active carbon site; red and pink balls refer to O, and H, respectively; the molecule under the graphene sheet represents TMX_2, where blue and yellow balls refer to TM and X. Free energy diagram of representative structures in each group of (B) OER and (C) ORR in 4e-transfer pathways when the electrode is 0V. (D) Free energy diagram of representative structures in each group of 2e-transfer pathways.

We firstly discuss the 4-electron transfer ORR and OER. Figure 3B-C and Figure S2-S3 show the free energy diagrams of ORR and OER on G/TMX_2 with the lowest overpotentials. For OER, nearly all the G/TMX_2 structures are uphill at an electrode potential of 0V except for G/MnF_2 and $G/MnBr_2$ structures. For most of the G/TMX_2 structures the rate limiting step is the first electron transfer to absorb water molecule to form HO*, except for G/TMX_2 (G/VF_2, G/VF_2, G/VBr_2, $G/CrBr_2$, $G/CoBr_2$, and G/CoI_2) with their rate limiting step at the third electron transfer (the transformation of O* to HOO*). Our results show that the OER free energy change of G/VF_2, $G/CrCl_2$, $G/CrBr_2$ and G/VI_2

are very close to that of the ideal catalyst, indicating that these structures may have better catalytic performance than others in their own groups. Among all the structures, $G/CrBr_2$ has the lowest overpotential and may exhibit the best OER catalytic activity among all G/TMX_2 structures. Similarly, for ORR in acid solutions, the rate limiting step is the first electron transfer, $O_2^* + H^+ + e^- \rightarrow HOO^*$, which are consistent with the previous reports [34,35]. Among all G/TMX_2 structures, $CrBr_2$ absorbed graphene shows the lowest overpotential for ORR and thus is the best ORR catalyst among them. Overall, $CrBr_2$ absorbed graphene performs the best catalytic activity in both OER and ORR process, indicating that the structure of $G/CrBr_2$ may be a promising bifunctional OER and ORR catalyst.

For 2-electron pathways (Figure 3D and Figure S4), among them, both G/TiX_2 and G/CrX_2 could occur spontaneously, but G/MnX_2 and G/CuX_2 cannot lead to spontaneous reaction both in 2e- and 4e-transfer pathways. In particular, the overpotentials of G/CoF_2, $G/TiCl_2$, $G/CrBr_2$ and G/CoI_2 are much closer to the ideal catalysts of their own group. These catalysts are better in catalyzing the production of H_2O_2 compared with the other structures in their own groups. Among all the structures, G/CoF_2 is one of the best catalysts (Figure 3dD) for H_2O_2. Compared with the best Pd catalysts with an overpotentials of 0.08V[36], G/CoF_2 is even lower than Pd catalysts, indicating that it could have better catalytic activity than Pd.

3.2 Scaling factor and descriptors for volcano relationship

To screen highly active catalysts from the candidate materials, it is necessary to find descriptors that well describe the catalytic activities of the halide-adsorbed graphene. Figure 4A shows the plots of ΔG_{HOO*} vs ΔG_{HO*} (where ΔG is the free energy of adsorption) for the active sites with the lowest overpotentials of ORR and OER on G/TMX_2 structures in 4-electron transfer pathways. From Figure 4a, a linear relationship is expected between ΔG_{HOO*} and ΔG_{HO*}, which can be used to calculate the lower limit of ORR and OER overpotentials of G/TMX_2 structures are determined to be 0.31V.

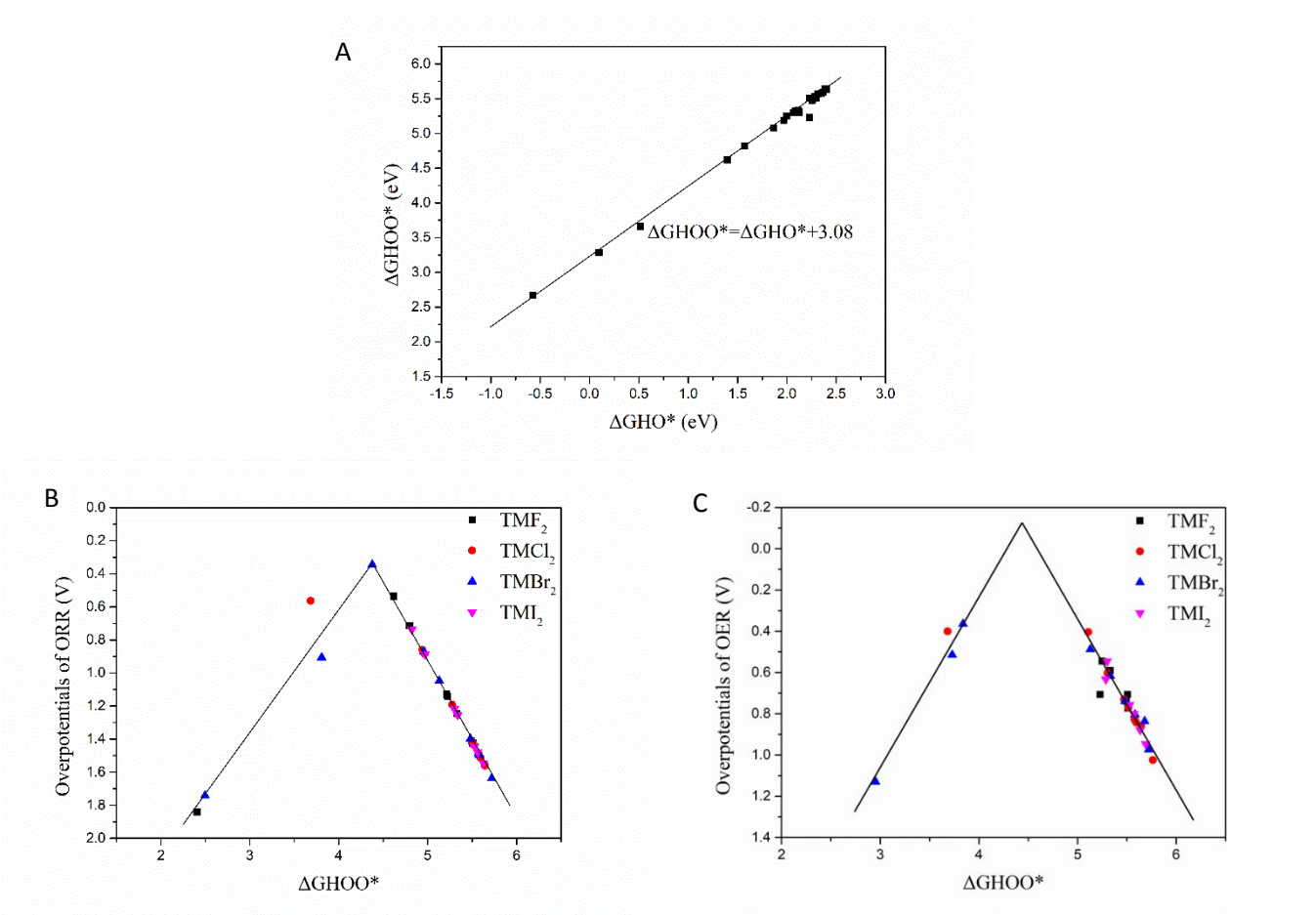

Figure 4. (A) Absorption energy of OOH* versus that of OH* on $G/TMBr_2$ for 4-electron transfer pathways. The lowest (B) ORR and (C) OER overpotentials for $G/TMBr_2$ versus the absorption energy of OOH* in 4-electron transfer pathways.

To find out the most active sites on the TMX_2 absorbed graphene, we took ΔG_{HOO*} as a descriptor to describe the relationship between ΔG_{HOO*} and the overpotentials. Figure 5B and C shows the overpotentials η^{OER} and η^{ORR} versus descriptor, ΔG_{HOO*}. The lowest OER and ORR overpotentials for 4-electron transfer pathways are listed in Table S3. As shown in Figure 4B, C, there are volcano relationships and the $G/CrBr_2$ sits on the top of the volcano (ORR ~ 0.35 V), and also shows the lowest OER overpotentials (OER ~ 0.36V) among the $G/TMBr_2$. These predicted OER and ORR overpotentials are much lower than those of the noble metal catalysts (OER on RuO_2-rutile is 0.42 V[2] and ORR on Pt is 0.45V[3]). Thus, $G/CrBr_2$ structure are identified as the most effective bifunctional catalyst for both OER and ORR among all the G/TMX_2 structures.

3.3 Intrinsic descriptors and role of electric field induced by buried salts

Although the above descriptor can well predict the activities of the G/TMX_2, it is highly desirable to find an intrinsic descriptor that correlate the G/TMX_2 structures with the catalytic activities. It has been shown that the TM ions carry different charge in different G/TMX_2 structures due to the interactions with the haloid elements and graphene (Table S1 and S3). The TM ions with strongly positive charge could induce an interfacial electric field[37], which significantly influences the adsorption of intermediates and thus ORR/OER occurring on the surface of the graphene. We therefore consider the electrostatic force as an intrinsic descriptor to describe the catalytic activities. According to the Coulomb's law, the electrostatic interaction force between TMX_2 and intermediates (F_a) may be related to the charge that the TM carries (Q) and the distance between TM and graphene surface (R). Hence, we defined the new descriptor as

$$F_a = \frac{Qe}{R^2} \qquad (4)$$

where e is the charge of an electron.

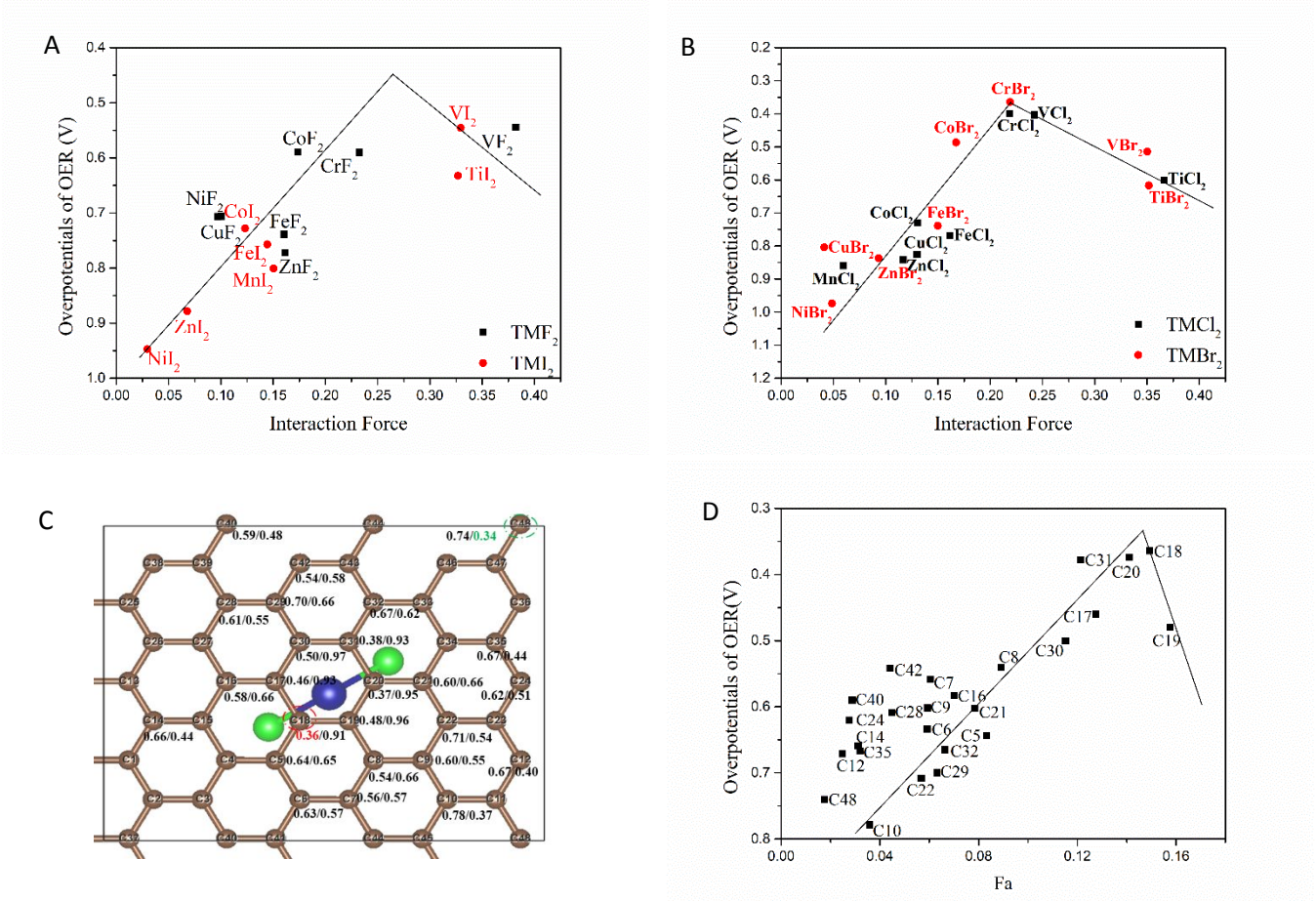

Figure 5. The electrostatic interaction force between TMX_2 and intermediates (F_a) of (A) Group G/TMF_2 and G/TMI_2 and (B) Group $G/TMBr_2$ and $G/TMCl_2$ vs overpotentials of OER. (C) Sites at which ORR and OER could occur. The numbers are the values of overpotentials (η_{OER}/η_{ORR}); the red numbers and cycles represent the lowest overpotential of OER on this site, and the green numbers and cycles represent the lowest overpotential of ORR on this site, respectively. (D) The overpotentials of OER on catalytic sites near the Cr ion of $CrBr_2$ as a function of the electrostatic force Fa.

The overpotentials were plotted as a function of new descriptor in Figure 5A and B. To more clearly show the relationship for different G/TMX_2 structures, we divide them into 2 groups according to the adsorption energy of TMX_2 on graphene (Table S7 and Figure S5). One group includes G/TMF_2 and G/TMI_2 with the adsorption energy around 9eV, and the other consist of G/$TMCl_2$ and G/$TMBr_2$ with the adsorption energy around -0.5eV. There is a volcano relationship between F_a and the overpotentials of OER. At the summit of the volcano plot is G/$CrBr_2$, from which the best catalysts are predicted.

To get more insight into the role of electrical field in OER, we further calculated the distance between the TM ion and the active sites (carbon atoms) in G/$CrBr_2$, the best bifunctional catalyst identified so far. For OER on G/$CrBr_2$, the relatively low overpotentials locate at C18, C20 and C31 with overpotentials of 0.36V, 0.37V and 0.38V, respectively. All the sites for ORR and OER are marked in Figure 5C. We measured the distance (R) from the carbon atoms to TM ion (Cr) of the G/$CrBr_2$ structure (Table S8**)**. When the distance between Cr and C is less than 4Å, the catalytic activity shows a volcano relationship with Qe/R^2 (Figure 5D), indicating that the electric field induced by the adsorbed molecule dominates the OER on the graphene surface. However, when the distance between Cr and C is larger than 4Å, the effect of electrical field becomes very weak or even disappear. A larger model (G/$CrBr_2$) with 80 atoms shows the similar trend (Figure S6).

Unlike the OER active sites that usually locate near TMX_2, those mostly active sites for ORR are far from the metal ion and therefore do not form the distinctive volcano relationship with the electrostatic force Fa (Figure S7). To understand this phenomenon, we calculated the charge density on the graphene structures and found that all the active sites are located in the part with positive charge distribution (Figure S8), which is consistent with the previous results[21].

3.4 Spin-down d band center for determining the catalytic activities

For metallic catalysts, d-band center[38,39] (denoted as ε) has been successfully used to describe the catalytic activity of transition metal catalysts. According to the d-band center model, the higher the d-band center, the stronger the adsorption. However, the adsorption behavior on some material surfaces cannot be well explained from the d-band center.[40-42] Since the d-orbitals' spin states can be divided into spin-up and spin-down states for 3d transition metals, we take spin-down d-orbitals into consideration. Similarly, we define the spin-down d-band center (denoted as ε_{down}) as a descriptor for the G/$TMBr_2$. The ε_{down} was calculated by

$$\varepsilon_{down} = \frac{\int_{-\infty}^{+\infty} x\rho(x)\mathrm{d}x}{\int_{-\infty}^{+\infty} x\mathrm{d}x} \qquad (5)$$

where x is the energy of spin-down d-electrons and ρ is the density of state of spin-down d-electrons. The equation of ε_{down} is similar to the calculation method for ε, but the difference between them is that the DOS is the spin-down d-DOS. The calculation results show that there is a nearly proportional relationship between ε-down and ε, as shown in Figure S9. Since the metal ions in halide-adsorbed graphene play an important role in the catalytic activity, we use ε_{down} as a descriptor to describe the relationship between overpotentials and ε_{down}. As shown in Figure 6, the overpotential-ε_{down} plot can be divided into two regions: for $\varepsilon_{down} < 0$, there are very large overpotentials for both OER and ORR, indicating that the catalytic activities are very weak. When $\varepsilon_{down} > 0$, an excellent linearity can be observed between the overpotential and ε_{down} for both OER and ORR. The overpotentials nearly linearly decrease with increasing $\varepsilon_{down,}$ for $\varepsilon_{down} > 0$, suggesting that the best catalysts could be found by searching for the materials with the lowest spin-down d-orbitals of TM (Figure S10). A larger ε_{down} means that the most spin down d orbitals are with high level energy, and the materials with larger ε_{down} needs less energy to absorb the intermediates in the catalytic process. Therefore, increasing ε_{down} of G/TMX_2 could enhance the bifunctional catalytic activities for both OER and ORR.

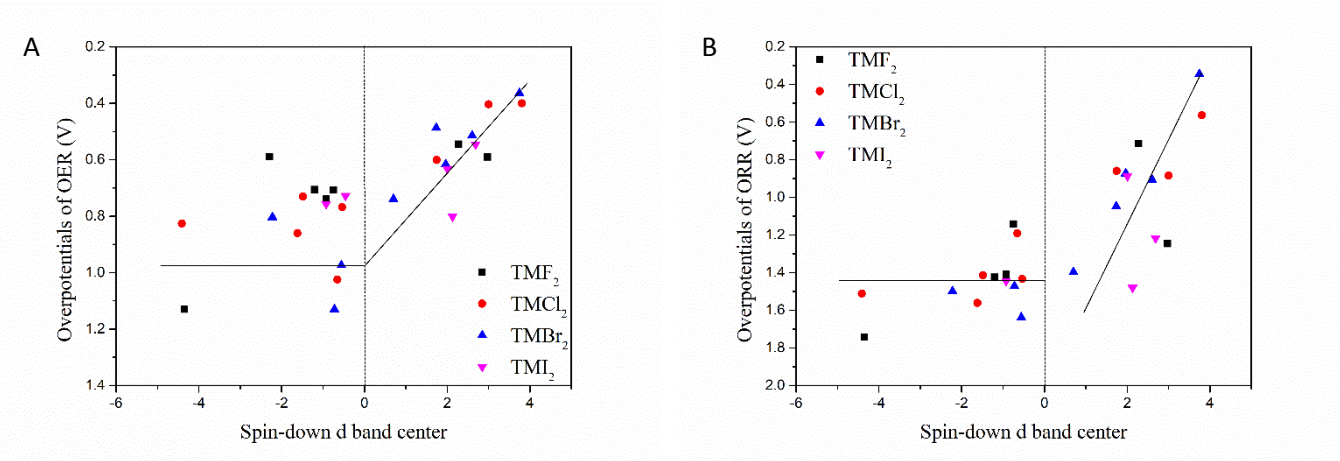

Figure 6. Spin-down d band center ε_{down} of the G/$TMBr_2$ versus the overpotentials of (A) OER and (B) ORR

4. Conclusion

We have calculated the overpotentials of OER and ORR on TMX_2 (TM = Ti, V, Cr, Mn, Fe, Co, Ni, Cu, and Zn; X = F, Cl, Br, I) absorbed graphene and introduced intrinsic descriptors to describe the catalytic activities of TMX_2 absorbed graphene. A design principle has been established to describe the relationship between the catalytic activates and the descriptor. The catalytic activity of the G/TMX_2 are also associated with the spin-down d-band center. Among the TMX_2 absorbed graphene structures, G/$CrBr_2$ is identified to be the best bifunctional electrocatalysts for both OER and ORR with overpotentials of 0.36V and 0.35V in 4-electron pathways, respectively. G/CoF_2 is considered as the best electrocatalysts to facilitate H_2O_2 in 2-electron pathways with overpotentials of 0.03V. The high catalytic activities of the $CrBr_2$ absorbed graphene are originated from the synergistic effects of 3d transition metals, halogens adsorbed TMX_2 that leads to the charge redistribution and charge transfer between $CrBr_2$ and graphene. Our results would provide an approach for rational design of novel hybrid catalysts, which would work effectively and durably in acidic environments.

Conflicts of interest

There are no conflicts to declare.

Acknowledgement

We thank the National Key Research and Development Program of China (2017YFA0206500), National Natural Science Foundation of China (51732002, 51973174), Distinguished Scientist Program at BUCT (buctylkxj02), the Fundamental Research Funds for the Central Universities (3102019ZD0402), and US National Science Foundation (1561886 and 1662288) for the support of this research. Computational resources were provided by UNT high performance computing initiative.

References

1 C. Sealy, Materials Today, 2008, 11, 65-68.
2 J. K. Nørskov, J. Rossmeisl, A. Logadottir, L. Lindqvist, J. R. Kitchin, T. Bligaard and H. Jonsson, *The Journal of Physical Chemistry B*, 2004, 108, 17886-17892.
3 I. C. Man, H. Y. Su, F. Calle-Vallejo, H. A. Hansen, J. I. Martínez, N. G. Inoglu, J. Kitchin, T. F. Jaramillo, J. K. Nørskov and J. Rossmeisl, *ChemCatChem*, 2011, 3, 1159-1165.
4 K. Gong, F. Du, Z. Xia, M. Durstock and L. Dai, *Science*, 2009, 323, 760-764.
5 X.-K. Kong, C.-L. Chen and Q.-W. Chen, *Chemical Society Reviews*, 2014, 43, 2841-2857.
6 L. Qu, Y. Liu, J.-B. Baek and L. Dai, ACS nano, 2010, 4, 1321-1326.
7 X. Liu and L. Dai, *Nature Reviews Materials*, 2016, 1, 16064.
8 Y. Jiao, Y. Zheng, M. Jaroniec and S. Z. Qiao, *Chemical Society Reviews*, 2015, 44, 2060-2086.
9 L. Dai, Y. Xue, L. Qu, H.-J. Choi and J.-B. Baek, *Chemical reviews*, 2015, 115, 4823-4892.
10 L. Zhang, J. Niu, L. Dai and Z. Xia, *Langmuir*, 2012, 28, 7542-7550.
11 S. Wang, D. Yu, L. Dai, D. W. Chang and J.-B. Baek, *ACS Nano*, 2011, 5, 6202-6209.

12 A. Shen, W. Xia, L. Zhang, S. Dou, Z. Xia and S. Wang, *Nanotechnology*, 2016, 27, 185402.
13 Z. Zhao, L. Zhang and Z. Xia, *The Journal of Physical Chemistry C*, 2016, 120, 2166-2175.
14 G. Colherinhas, E. E. Fileti and V. V. Chaban, *Physical Chemistry Chemical Physics*, 2015, 17, 17413-17420.
15 C. Yang, J. Chen, X. Ji, T. P. Pollard, X. Lü, C.-J. Sun, S. Hou, Q. Liu, C. Liu and T. Qing, *Nature*, 2019, 569, 245.
16 G. Cassone, P. V. Giaquinta, F. Saija, and A. M. Saitta, The Journal of Physical Chemistry B, 2014, 118, 12717-12724.
17 G. Cassone, P. V. Giaquinta, F. Saija and A. M. Saitta, *The Journal of chemical physics*, 2015, 142, 054502.
18 F. Creazzo, D. R. Galimberti, S. Pezzotti and M. P. Gaigeot, *The Journal of chemical physics*, 2019, 150, 041721.
19 Z. Zhao, M. Li, L. Zhang, L. Dai and Z. Xia, *Advanced Materials*, 2015, 27, 6834-6840.
20 C. Y. Lin, L. Zhang, Z. Zhao and Z. Xia, Advanced Materials, 2017, 29, 1606635.
21 C. Zhu, J. Yun, Q. Wang and G. Yang, *Applied Surface Science*, 2018, 435, 329-337.
22 G. Kresse and J. Furthmüller, *Computational materials science*, 1996, 6, 15-50.
23 G. Kresse and J. Furthmüller, *Physical Review B*, 1996, 54, 11169.
24 P. E. Blöchl, *Physical review B*, 1994, 50, 17953.
25 J. P. Perdew, K. Burke and M. Ernzerhof, *Physical Review Letters*, 1996, 77, 3865.
26 I. Solovyev, P. Dederichs and V. Anisimov, *Physical Review B*, 1994, 50, 16861.
27 K. Kinoshita, Electrochemical oxygen technology, John Wiley & Sons, 1992.
28 B. C. Steele and A. Heinzel, in Materials For Sustainable Energy: A Collection of Peer-Reviewed Research and Review Articles from Nature Publishing Group, World Scientific, 2011, pp. 224-231.
29 Z. Zhao, L. Zhang, C. Y. Lin and Z. Xia, Carbon-Based Metal-Free Catalysts: Design and Applications, 2018, 1, 1-33.
30 J. K. Nørskov, J. Rossmeisl, A. Logadottir, L. Lindqvist, J. R. Kitchin, T. Bligaard and H. Jonsson, *The Journal of Physical Chemistry B*, 2004, 108, 17886-17892.
31 M. Li, L. Zhang, Q. Xu, J. Niu and Z. Xia, *Journal of Catalysis*, 2014, 314, 66-72.
32 F. Calle-Vallejo, J. I. Martinez and J. Rossmeisl, *Physical Chemistry Chemical Physics*, 2011, 13, 15639-15643.
33 J. Rumble, CRC handbook of chemistry and physics, CRC press, 2017.
34 R. A. Sidik, A. B. Anderson, N. P. Subramanian, S. P. Kumaraguru and B. N. Popov, *The Journal of Physical Chemistry B*, 2006, 110, 1787-1793.
35 Y. Okamoto, Applied Surface Science, 2009, 256, 335-341.
36 A. Verdaguer-Casadevall, D. Deiana, M. Karamad, S. Siahrostami, P. Malacrida, T. W. Hansen, J. Rossmeisl, I. Chorkendorff and I. E. Stephens, *Nano Letters*, 2014, 14, 1603-1608.
37 T. Meng, Y.-N. Hao, J. Qin and M. Cao, *ACS Sustainable Chemistry & Engineering*, 2019, 7, 4657-4665.
38 B. Hammer and J. Norskov, *Nature*, 1995, 376, 238.
39 A. Ruban, B. Hammer, P. Stoltze, H. L. Skriver and J. K. Nørskov, *Journal of Molecular Catalysis A: Chemical*, 1997, 115, 421-429.
40 M. Qiu, Z. Fang, Y. Li, J. Zhu, X. Huang, K. Ding, W. Chen and Y. Zhang, *Applied Surface Science*, 2015, 353, 902-912.
41 F. Calle-Vallejo, J. Martínez, J. M. García-Lastra, J. Rossmeisl and M. Koper, *Physical review letters*, 2012, 108, 116103.
42 H. Xin and S. Linic, *The Journal of Chemical Physics*, 2010, 132, 221101.